IOP FTC
IOP PUBLISHING JOURNAL OF PHYSICS: CONDENSED MATTER
J. Phys.: Condens. Matter **25** (2013) 102202 (6pp) doi:10.1088/0953-8984/25/10/102202

FAST TRACK COMMUNICATION

Development of a bond-valence based interatomic potential for $BiFeO_3$ for accurate molecular dynamics simulations

Shi Liu, Ilya Grinberg and Andrew M Rappe

The Makineni Theoretical Laboratories, Department of Chemistry, University of Pennsylvania, Philadelphia, PA, 19104-6323, USA

E-mail: rappe@sas.upenn.edu

Received 17 December 2012, in final form 23 January 2013
Published 12 February 2013
Online at stacks.iop.org/JPhysCM/25/102202

Abstract
We present an atomistic potential for $BiFeO_3$ based on the principles of bond-valence (BV) and bond-valence vector (BVV) conservation. The validity of this model potential is tested for both canonical ensemble (*NVT*) and isobaric–isothermal ensemble (*NPT*) molecular dynamics (MD) simulations. The model reproduces the ferroelectric-to-paraelectric phase transition in both *NVT* and *NPT* MD simulations and the temperature dependence of the local structure in $BiFeO_3$. The calculated domain wall energies for 71°, 109°and 180° walls agree well with density functional theory results. The success of our simple model potential for $BiFeO_3$ indicates that BV and BVV conservation provides a firm basis for the development of accurate atomistic potentials for complex oxides.

(Some figures may appear in colour only in the online journal)

$BiFeO_3$ (BFO) is a multiferroic perovskite oxide with high Curie and Neel temperatures ($T_C \approx 1100$ K and $T_N \approx 643$ K) [1, 2]. Recently, it has attracted intense attention, both experimentally and theoretically, due to its potential technological applications [3–10]. First-principles density functional theory (DFT) calculations have been applied to study the structural, electronic, magnetic, and ferroelectric properties of $BiFeO_3$ [11–15]. However, conventional first-principles methods are limited due to their large computational cost. Bellaiche *et al* [16] recently developed an effective Hamiltonian scheme for $BiFeO_3$, which enables the computational investigation of finite-temperature properties via Monte Carlo simulations [17, 18]. Despite this success, there is still a strong need for a true atomistic potential that could reproduce the full dynamical behavior of $BiFeO_3$ at finite temperature. However, the development of general atomistic potentials for ferroelectric oxides has proven difficult due to the complex nature of various metal–oxygen bonds [19].

We recently developed a classical potential for $PbTiO_3$ [20] based on the bond-valence and the bond-valence vector conservation principles [21, 22]. The bond-valence conservation principle states that each atom i prefers to have the total bond-valence of its bonds equal to its atomic valence, $V_{0,i}$. The actual atomic valence V_i for atom i can be calculated by summing over the individual bond valences V_{ij} for bonds between the atom and its nearest neighbors. It has been shown in many inorganic compounds that the bond-valence (BV) can be modeled with an inverse power-law correlation between the bond length and the bond-valence [23, 24] given in equation (1).

$$V_{ij} = \left(\frac{r_{0,ij}}{r_{ij}}\right)^{C_{ij}}, \quad (1)$$

where $r_{0,ij}$ and C_{ij} are Brown's empirical parameters and are readily available for many atomic pairs [21]. The bond-valence vector (BVV), $\mathbf{V}_{ij}$, is defined as a vector directed along the bond line with magnitude equal to the

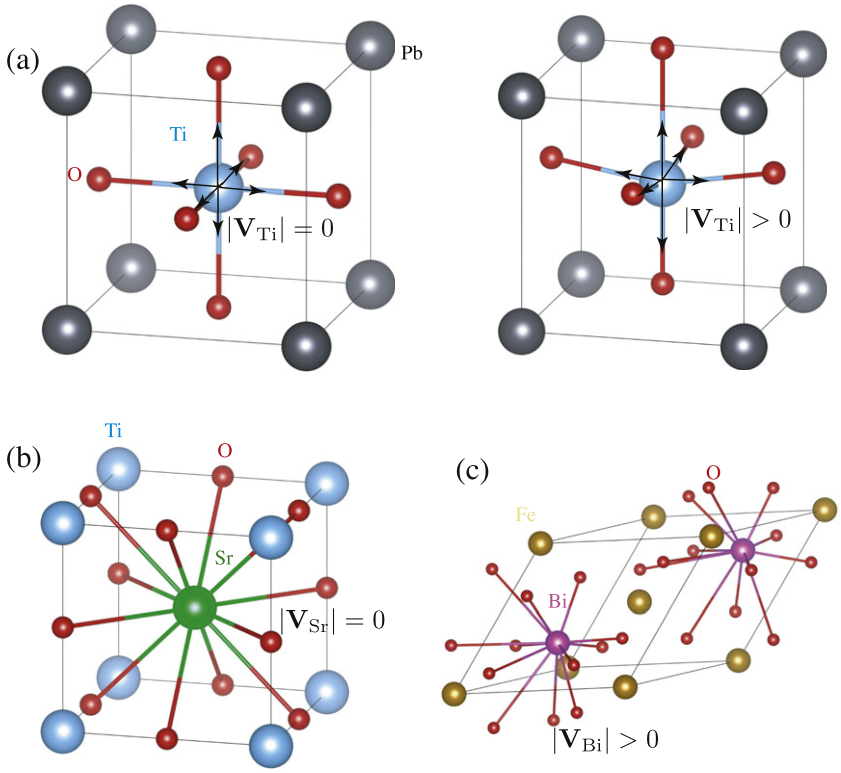

Figure 1. Schematic representation of bond-valence vector summation. (a) Cubic $PbTiO_3$ and tetragonal $PbTiO_3$; (b) cubic $SrTiO_3$; (c) ground state $BiFeO_3$.

scalar bond-valence. The bond-valence vector summation (BVVS), $\mathbf{V}_i$, is the vector sum of individual $\mathbf{V}_{ij}$ [22]. As shown in figure 1, the BVVS serves as a measure of local symmetry breaking. We therefore propose that each atom is assumed to have a desired length of BVVS, $|\mathbf{V}_{0,i}|$. The bond-valence vector conservation principle applies not only to a vast number of materials where BVVS $= 0$ is preferred but also to materials exhibiting noncentrosymmetric atomic environments due to electronic distortions, such as the second-order Jahn–Teller distortion for d^0 cations (Ti^{4+} and Nb^{5+}) and lone-pair driven distortion of Pb^{2+} and Bi^{3+}. The improved model potential of $PbTiO_3$ has been applied to both canonical ensemble (*NVT*) and isobaric-isothermal ensemble (*NPT*) molecular dynamics (MD) simulations. In this paper, we demonstrate that our BV model can be generalized to other materials by developing an atomistic potential for $BiFeO_3$.

The total interatomic potential for BFO is given by:

$$E = E_c + E_r + E_{\mathrm{BV}} + E_{\mathrm{BVV}} \tag{2}$$

$$E_c = \sum_{i<j} \frac{q_i q_j}{r_{ij}} \tag{3}$$

$$E_r = \sum_{i<j} \left(\frac{B_{ij}}{r_{ij}}\right)^{12} \tag{4}$$

$$E_{\mathrm{BV}} = \sum_i S_i (V_i - V_{0,i})^2, \tag{5}$$

$$E_{\mathrm{BVV}} = \sum_i D_i (\mathbf{V}_i^2 - \mathbf{V}_{0,i}^2)^2 \tag{6}$$

where E_c is the Coulomb energy, E_r is the short-range repulsive Lennard-Jones energy, E_{BV} is the bond-valence energy, and E_{BVV} is the bond-valence vector energy. The E_{BV} and E_{BVV} will be minimized when all the ions in a crystal structure have positions satisfying the desired BVS and BVVS. We note that we recently justified the BV energy quantum mechanically in a framework of a tight-bonding model, showing that the BV energy term is formally equivalent to a second moment bond-order potential, and the BVVS term is linked to the fourth moment of the local density of states [20]. Those derivations provide a firm physical basis for our BV model. The potential parameters obtained from the fitting are: charges q_i, scaling factors S_i and D_i for each species and short-range repulsion parameters, B_{ij}.

We use the simulated annealing global optimization method to optimize potential parameters by fitting a database of *ab initio*-derived structural energy differences and atomic forces. The electronic structure is calculated with the local density approximation (LDA) plus Hubbard U parameter as implemented in the QUANTUM-ESPRESSO [25] package. We use the 40 atom supercell as the reference structure. The Brillouin zone is sampled using a $4 \times 4 \times 4$ Monkhorst–Pack k-point mesh [26]. We use norm-conserving pseudopotentials [27] generated using OPIUM [28] with a plane-wave energy cutoff of 50 Ryd. The initial database contains the ground-state ferroelectric rhombohedral ($R3c$) structure, strained $R3c$ structures, paraelectric rhombohedral ($R\bar{3}c$), strained $R\bar{3}c$ structures, and randomly chosen orthorhombic structures with various lattice constants. The

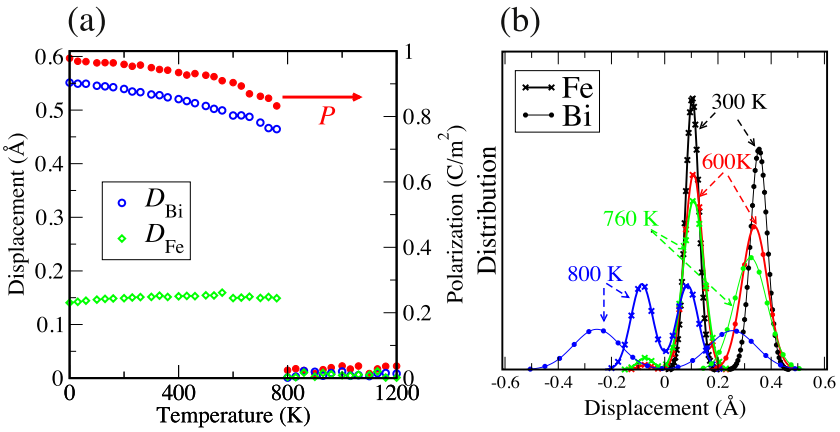

Figure 2. Temperature-dependent properties of $BiFeO_3$ obtained from *NVT* simulations. (a) Spontaneous polarization and average atomic displacements of Bi and Fe along the [111] axis for $BiFeO_3$. (b) Probability distributions of atomic displacements along [100] axis. The atomic displacements along [010] and [001] show similar distributions.

Table 1. Optimized potential parameters for $BiFeO_3$.

				B_{ij} (Å)				
	q_β (e)	S_β (eV)	D_β	Fe	Bi	O	$V_{0,\beta}$	$\mathbf{V}_{0,\beta}$
Fe	1.937 53	0.840 65	—	—	1.701 39	1.48 115	3.00	0.017 98
Bi	1.777 06	0.703 13	0.767 98	—	1.785 29	1.770 85	3.00	0.873 73
O	−1.238 20	0.672 13	4.500 44	—	—	1.391 14	2.00	0.328 66

optimized force field obtained from each simulated annealing run is used to run both constant-volume and constant-stress MD simulations to generate equilibrium structures at various temperatures, the energies and atomic forces of which are then added to the fitting database. We also used the 109° domain wall structure found by Lubk *et al* [37] in the database to ensure correct domain wall energies. The parameterization process is continued until the force field correctly reproduces the DFT energies and atomic forces of structures sampled by MD simulations.

Table 1 presents the optimized potential parameters. Brown's empirical parameters $r_{0,ij}$ are tuned until $V_{0,i}$ values for Bi, Fe and O in the ground-state structure are equal to their respective atomic valences ($C_{BiO} = 6.0$, $r_{0,BiO} = 2.071$ Å, $C_{FeO} = 5.117$, $r_{0,FeO} = 1.756$ Å). The value of desired BVVS is then calculated with the modified empirical parameters. The validity of the potential is first tested via constant-volume MD simulations at various temperatures with lattice constants fixed to experimental values [9]. For these simulations, we used a 5120 atom rhombohedral supercell ($a = b = c = 44.64$ Å, $\alpha = \beta = \gamma = 60°$) and the Nosé–Hoover thermostat to control the temperature. Figure 2(a) shows the temperature dependence of polarization along the [111] axis. The simulations show a ferroelectric-to-paraelectric first-order phase transition at $T_C = 760$ K. Analysis of local displacements (figure 2(b)) shows that at $T < T_C$, all displacements are only along the [111] direction. At $T > T_C$, the local displacements are non-zero but are evenly split between the positive and negative directions, resulting in no net polarization. This behavior is characteristic of the order–disorder phase transition. The magnitude of the local displacements decreases with temperature, which is characteristic of the displacive phase transition. We therefore conclude that the phase transition is of the mixed order–disorder and displacive character, as is typical for ferroelectrics.

We then used the potential in *NPT* simulations. The external stress is maintained at 0.1 MPa by the Parrinello–Rahman barostat. We used a 2560 atom perovskite-type orthorhombic supercell as the starting structure. Figure 3 depicts the evolution of polarization and atomic displacements with temperature. At low temperature, all three components of polarization, P_x, P_y and P_z, have significant values with small fluctuation, such that the overall polarization points toward the [111] direction. As the temperature increases, the magnitude of the polarization decreases. At high temperature (700 K), P_x, P_y and P_z all become zero, indicating a paraelectric structure. Therefore, the T_C obtained from *NPT* MD simulation is 660 K. This underestimates the experimental T_C of 1100 K. Such underestimation is consistent with the previously found underestimation of T_C in *NPT* BVMD $PbTiO_3$ simulations [20]. The difficulty of reproducing experimental T_C appears to be a general feature for both atomistic simulation using interatomic potential [29, 30] and the effective Hamiltonian scheme [31–34]. We believe that this systematic error is partly due to the use of LDA functional in potential parameterization. DFT calculations with the LDA functional are known to underestimate the experimental lattice constants and P values. Since in perovskites T_C scales as P^2, smaller P magnitude leads to underestimation of theoretical

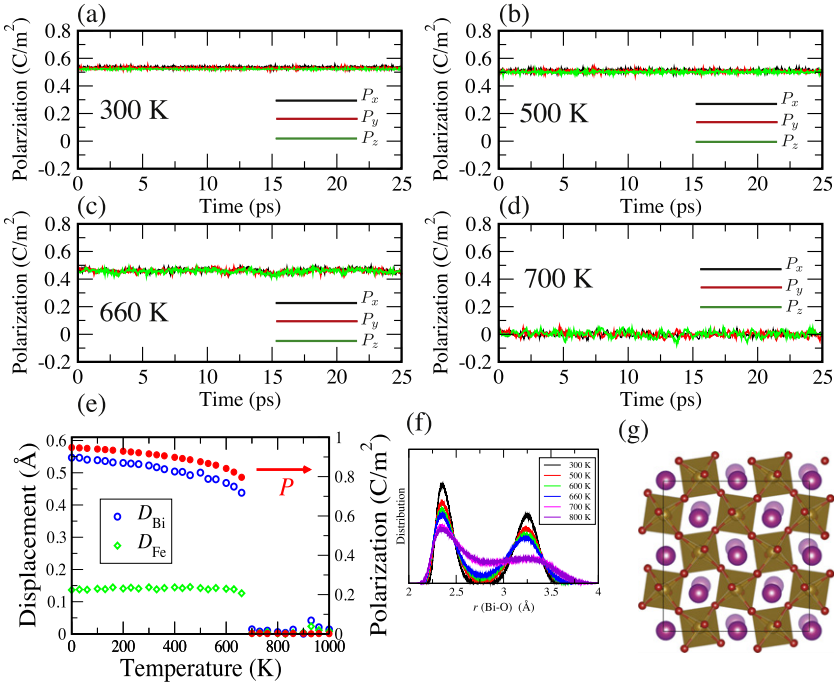

Figure 3. Temperature-dependent properties of $BiFeO_3$ obtained from *NPT* simulations. (a)–(d) Evolution of polarization along Cartesian axes. (e) Spontaneous polarization and atomic displacements along the [111] axis as a function of temperature. (f) Pair distribution function for Bi–O atomic pair as a function of temperature. (g) Oxygen octahedral tilting in $BiFeO_3$ at 700 K along *c* axis.

T_C. The underestimation of T_C may also be partially due to an imperfect representation of the DFT potential by the atomistic force-field model. Since our bond-valence model is essentially a simplified fourth-moment bond-order potential, introducing new energy terms that utilize higher moments may further improve its performance.

Analysis of local structure shows that below T_C the displacements of Fe^{3+} ions with respect to the center of their oxygen octahedra do not change with temperature significantly. On the other hand, the displacement of Bi^{3+} shows a stronger temperature dependence, with a strong decrease as temperature increases. This agrees with previous experimental studies [35, 36] which found that the shift of Bi^{3+} makes the main contribution to the temperature changes of the electric polarization of $BiFeO_3$. It is also found that the pair distribution function (PDF) for Bi–O atomic pair exhibits two well separated peaks below T_C, and then become more dispersed above T_C. This indicates the change of the coordination number of Bi during phase transition, which supports the *R3C* to *Pbnm* phase transition reported previously [36]. The time-averaged structure of the paraelectric phase (averaged with 500 structures obtained from a 20 ps MD simulation) is close to the structure of $GdFeO_3$, which shows octahedral tilting of $a^-a^-b^+$, typical for perovskite with space group *Pbnm* (figure 3(g)). This further supports the assignment of *Pbnm* as the space group of the paraelectric phase.

Domain structure and dynamics play important roles in ferroelectric switching, photovoltaic effects and other phenomena intensely studied in $BiFeO_3$. To further test the potential and its applicability to the study of BFO domain walls, we calculate the energies of 71°, 109°, and 180° domain walls. The domain wall energy is estimated using:

$$E_{DW} = \frac{E_N - E_{bulk}}{S_{DW}} \tag{7}$$

where E_N is the energy of the supercell containing the domain wall, E_{bulk} is the energy of the bulk $BiFeO_3$ supercell of the same size, and S_{DW} is the domain wall area. For BFO, the DW structure is particularly interesting, as recent DFT calculations by Diéguez *et al* [38] found that several local minima are possible for the domain walls with up to factor of three difference in DW energy for the same DW orientation, compared to the values reported by Lubk *et al* [37]. The three low-energy and three high-energy DW structures found by Diéguez *et al* and Lubk *et al* therefore provide a stringent test of our potential, which as stated above, was parameterized using only the high-energy 109° wall.

To assess the accuracy of our BV potential, we carried out *NPT* simulations at 10 K using supercells shown in figure 4. The 71° wall was constructed with $6\sqrt{2} \times 2\sqrt{2} \times 4$ supercell with domain boundary in the (110) plane; the 109° domain wall was simulated with a $12 \times 2\sqrt{2} \times 2\sqrt{2}$ supercell with the boundary in (100) plane and polarization vector changing from $[1\bar{1}\bar{1}]$ to [111] across the domain wall; a $6\sqrt{2} \times 2\sqrt{2} \times 4$ supercell was used for constructing the 180° domain wall with boundary in the (110) plane. We found DW energies of 372 mJ m^{-2}, 232 mJ m^{-2}, 1032 mJ m^{-2} for the 71°, 109° and 180° high-energy walls, respectively. For the low-energy DWs, we found 156, 34 and 110 mJ m^{-2} for the 71°, 109° and 180° walls. These values compare favorably with 363, 205, 829, 167, 62 and 82 mJ m^{-2} DW

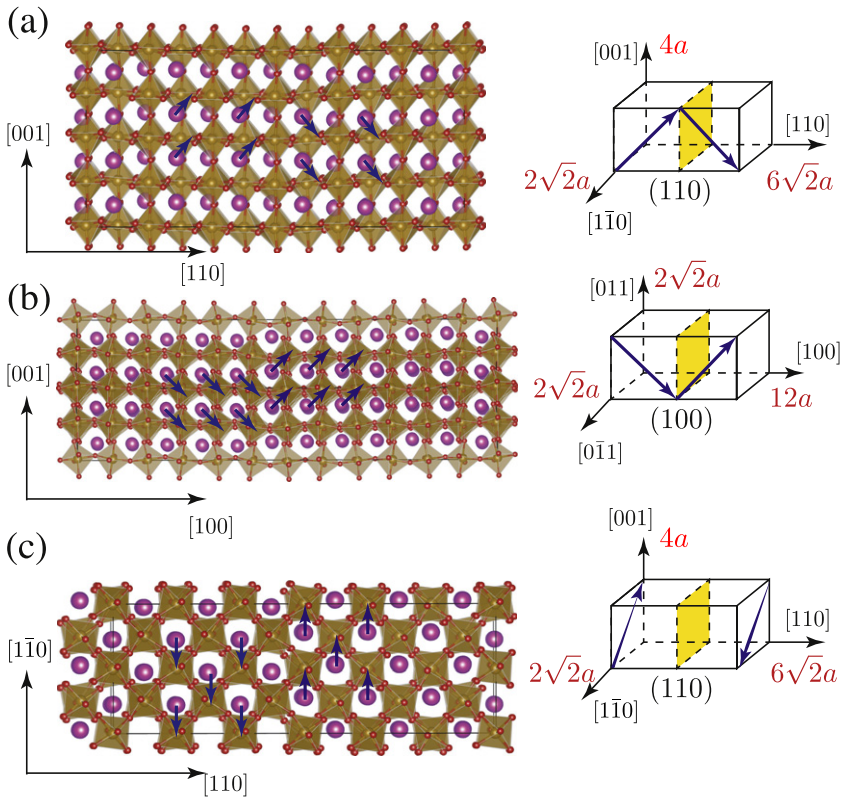

Figure 4. Simulated domain wall structures using the BV potential of $BiFeO_3$. (a) 71°; (b) 109°; (c) 180°. Dimensions of each supercell are given in units of the lattice constant a. The blue arrow represents the direction of polarizations.

energies obtained by the corresponding DFT calculations [37, 38]. The agreement between DFT and atomistic potential values is quite good and indicates that our atomistic potential accurately reproduces the $BiFeO_3$ potential energy surface. We emphasize once again that this agreement was achieved while only using the high-energy 109° structure in potential parameterization and is due to the firm physical basis of the potential.

In this work, we present an atomistic interatomic potential for $BiFeO_3$ based on the bond-valence and the bond-valence vector conservation principles. This model potential reproduces the ferroelectric to paraelectric phase transition and the temperature dependence of local cation displacements in $BiFeO_3$ in both *NVT* and *NPT* simulations. The calculated energies of various domain walls are also in agreement with DFT results. We believe that the bond-valence model approach achieves a balance between efficiency, accuracy, and transferability and we therefore expect that this type of interatomic potential will be applicable to a broad range of oxides.

SL was supported by the NSF through Grant CBET-1159736. IG was supported by the Office of Naval Research, under grant N00014-12-1-1033. AMR was supported by the Department of Energy under grant DE-FG02-07ER46431. Computational support was provided by the US DOD through a Challenge Grant from the HPCMO. SL acknowledges O Diéguez for sharing information of domain wall structures.

References

[1] Bhide V G and Multani M S 1965 *Solid State Commun.* **3** 271
[2] Moreau J M, Michel C, Gerson R and James W J 1971 *J. Phys. Chem. Solids* **32** 1315
[3] Wang J *et al* 2003 *Science* **299** 1719
[4] Fiebig M, Lottermoser T, Frhlich D, Goltsev A V and Pisarev R V 2002 *Nature Lond.* **419** 818
[5] Kimura T, Kawamoto S, Yamada I, Arima T and Takura Y 2003 *Nature Lond.* **426** 55
[6] Eerenstein W, Mathur N D and Scott J F 2006 *Nature* **442** 759–65
[7] Zhao T *et al* 2006 *Nature Lond.* **5** 823
[8] Ramesh R and Spaldin N A 2007 *Nature Mater.* **6** 21–9
[9] Catalan G and Scott J F 2009 *Adv. Mater.* **21** 2463
[10] Zeches R J *et al* 2009 *Science* **326** 977
[11] Neaton B, Ederer C, Waghmare U V, Spaldin N A and Rabe K M 2005 *Phys. Rev.* B **71** 014113
[12] Baettig P, Ederer C and Spaldin N A 2005 *Phys. Rev.* B **72** 214105
[13] Ravindran P, Vidya R, Kjekshus A and Fjellvåg H 2006 *Phys. Rev.* B **74** 224412
[14] Jung-Hoon L, Min-Ae O, Hyoung C J, Jong S Y and Hyun J M 2012 *J. Mater. Chem.* **22** 1667
[15] Prosandeev S, Kornev I A and Bellaiche L 2011 *Phys. Rev. Lett.* **107** 117602
[16] Kornev I A, Lisenkov S, Haumont R, Dkhil B and Bellaiche L 2007 *Phys. Rev. Lett.* **99** 227602
[17] Albrecht D, Lisenkov S, Ren W, Rahmedov D, Kornev I A and Bellaiche L 2010 *Phys. Rev.* B **81** 140401
[18] Prosandeev S, Kornev I A and Bellaiche L 2011 *Phys. Rev.* B **83** 020102

[19] Phillpot S R, Sinnott S B and Asthagiri A 2007 *Annu. Rev. Mater. Sci.* **37** 239
[20] Liu S, Takenaka H, Qi T, Grinberg I and Rappe A M 2012 arXiv:1211.5166
[21] Brown I D 2009 *Chem. Rev.* **109** 6858
[22] Harvey M A, Baggio S and Baggio R 2006 *Acta Crystallogr.* B **62** 1038
[23] Brown I and Shannon R 1973 *Acta Crystallogr.* A **29** 266
[24] Brown I and Wu K K 1976 *Acta Crystallogr.* B **32** 1957
[25] Giannozzi P *et al* 2009 *J. Phys.: Condens. Matter* **21** 395502
[26] Monkhorst H J and Pack J D 1976 *Phys. Rev.* B **13** 5188
[27] Rappe A M, Rabe K M, Kaxiras E and Joannopoulos J D 1990 *Phys. Rev. B Rapid Commun.* **41** 1227
[28] http://opium.sourceforge.net
[29] Sepliarsky M and Cohen R E 2002 *AIP Conf. Proc.* **626** 36
[30] Sepliarsky M, Asthagiri A, Phillpot S R, Stachiotti M G and Migoni R L 2005 *Curr. Opin. Solid State Mater. Sci.* **9** 107
[31] Zhong W, Vanderbilt D and Rabe K M 1994 *Phys. Rev. Lett.* **73** 1861
[32] Waghmare U and Rabe K 1997 *Phys. Rev.* B **55** 6161
[33] García A and Vanderbilt D 1998 *Appl. Phys. Lett.* **72** 2981
[34] Bellaiche L, García A and Vanderbilt D 2000 *Phys. Rev. Lett.* **84** 5427
[35] Palewicz A, Przeniosło R, Sosnowska I and Hewat A W 2007 *Acta Crystallogr.* B **63** 537
[36] Arnold D C, Knight K S, Morrison F D and Lightfoot P 2011 *Phys. Rev. Lett.* **107** 117602
[37] Lubk A, Gemming S and Spaldin N A 2009 *Phys. Rev.* B **80** 104110
[38] Diéguez O, Aguado-Puente P, Junquera J and Íñiguez J 2013 *Phys. Rev.* B **87** 024102